Temporal characteristics of monoenergetic electron beams generated by the laser wakefield acceleration

T. Ohkubo, A. Maekawa, R. Tsujii, T. Hosokai, K. Kinoshita, K. Kobayashi, and M. Uesaka
Nuclear Professional School, University of Tokyo, 2-22 Shirakata-shirane, Tokai, Naka, Ibaraki, Japan

A. Zhidkov and K. Nemoto
Central Research Institute of Electric Power Industry, 2-6-1 Nagasaka, Yokosuka, Kanagawa, Japan

Y. Kondo and Y. Shibata
Institute of Multidisciplinary Research for Advance Materials, Tohoku University, Sendai 980, Miyagi, Japan
(Received 27 June 2006; published 12 March 2007)

Pulse length of quasimonoenergetic electrons accelerated by the wakefield generated by 12 TW, 40 fs laser pulses in a gas jet is determined via spectral measurements using a bolometer to detect coherent transition radiation. A quasimonoenergetic electron beam with its mean energy $E = 21$ MeV, dispersion $\Delta E = 4$ MeV, total charge $q \sim 30$ pC, and the geometrical emittance 0.07π mm mrad is generated with high reproducibility. The averaged duration of only the quasimonoenergetic electron bunches peaked around 20 MeV is 130 ± 30 fs (FWHM), while it is 250 ± 70 fs (FWHM) for electron bunches with quasimonoenergetic distributions peaked around 4 MeV, at a distance of 180 mm far from the gas jet because of relatively large electron energy spread. Pulse elongation of the electron bunch with the quasimonoenergetic distribution after 180 mm path is 60–220 fs (FWHM). Therefore, the initial duration of the electron bunch at the gas-jet rear is expected to be less than 100 fs (FWHM).

DOI: 10.1103/PhysRevSTAB.10.031301 PACS numbers: 41.75.Jv, 52.38.Kd

Recent progress in the laser-plasma electron acceleration [the laser wakefield acceleration (LWFA)] [1,2] has brought about interest to detail characterization of dense and short electron beams generated by the laser wakefield. The temporal characteristic of such beams is of particular importance. The LWFA allows the jitterless generation of a set of bunches with their durations shorter than a typical relaxation time of the electronic subsystem of a condense matter [3]. A rate of nonadiabatic excitation of the electron subsystem by a time-dependent electric field is usually a Gaussian $\omega \sim \exp[-(\omega\tau)^2/2]$ with $\omega[\sim 10^{14}\ \mathrm{s}^{-1}]$ a typical frequency and τ the duration of the electric field, therefore for nonzero ω the bunch duration should be shorter than few tens of femtoseconds; for picosecond and subpicosecond electron beams ω is practically zero.

The self-injection of plasma electrons in the acceleration phase of the laser wakefield is a key part of the LWFA. One laser pulse can provide both the electron injection and the electron acceleration [1,2,4,5]. However, results of various numerical simulations of LWFA have shown that the femtosecond duration of driving laser pulse cannot guarantee the short duration of accelerated electrons [4,5]. The length of the electron bunch strongly depends on the way of their injection in the phase of laser wake for further acceleration. Although the mechanism of generation of accelerating laser wakefield by the ponderomotive force [6] is well known, various mechanisms of electron injection and their effect on the bunch length have yet to be understood. Therefore, only a direct measurement of electron bunch duration is a supreme test [7,8]. In Ref. [7], the bunch duration is estimated by the detection of THz radiation from the plasma boundary. Though there is no serious doubt in the result, this measurement cannot provide complete assurance that the radiation comes from the beam not from the plasma itself. In the present rapid communication, we perform a direct spectral measurement of the coherent part of transition radiation from a Ti foil produced by quasimonoenergetic electron beams accelerated by the wakefield of 17 TW, 40 fs laser pulses.

The experimental setup is shown in Fig. 1 (see also Ref. [2]). A supersonic pulsed helium gas jet settled in a vacuum chamber. The pulsed-slit gas jet is generated by a device consisting of a shock-wave-free slit nozzle and a solenoid fast pulse valve. The supersonic slit nozzle is designed to be forming the Mach number $M_e = 5.0$ flow for helium and has a 1.2 mm width and 4.0 mm length at the rectangular exit. The stagnation pressure of the valve can be varied up to 80 atm. With this pressure the density at the exit of the nozzle ranges up to $N_{\mathrm{He}} = 6 \times 10^{19}\ \mathrm{cm}^{-3}$. Uniform density distributions with the sharp boundary of the slit gas jet near the exit are verified by interferometry.

The 17 TW Ti:sapphire laser system generates with the pulse energy up to 650 mJ, 40 fs laser pulses at a fundamental wavelength of 790 nm with a 10 Hz repetition rate. The details of the laser system are described in Ref. [2]. In the present experiment, a 12 TW laser pulse with its diameter of 50 mm is delivered into the vacuum chamber and is focused to the gas jet by an off-axis parabolic mirror with a focal length of 178 mm. The focus position is 170 μm inside from the front edge of the slit nozzle

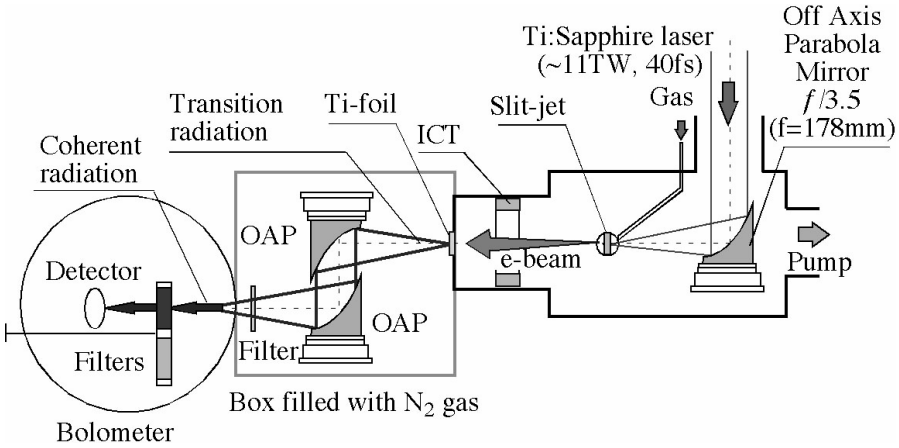

FIG. 1. Experimental setup for bunch duration measurement. Transition radiation emitted from Ti foil is detected by a bolometer.

boundary at a height of 1.5 mm from nozzle exit. The focal spot size is 6.0 μm in full width. The maximum laser intensity on the target is estimated to be $I = 4 \times 10^{19}$ W/cm^2. The contrast ratio of main pulse to the amplified spontaneous emission (ASE) prepulse preceding it at 150 ps is typically 5×10^{-7} at a fundamental wavelength. The nanosecond-scale prepulse, the pedestal can be controlled by tuning of the Pockels cells inside the regenerative amplifier.

To characterize and control the quasimonoenergetic electron beams in one shot, the measurements of plasma density dynamics by the shadowgraph, the spatial and energy distribution of the electrons, and the charge are performed. For the shadowgraph, a part of the laser pulse carrying about 1% energy of the main pulse is divided through a 2 μm thickness Pellicle window as a beam splitter. It is delivered into the target region in the direction of 90° from the laser propagation axis and is used as a probe pulse for the plasma diagnosis. The shadowgraph image of the plasma by this probe pulse provides information of the density structure of the evolving plasma with a time resolution ~100 fs; it is detected by a 14 bit charge coupled device (CCD) camera. A bandpass filter $\Delta\lambda =$ 20 nm at $\lambda = 790$ nm is put in front of the CCD to cut the plasma light. The polarization of the main laser pulse at the target is parallel to the probe beam axis. The synchronization of the probe pulse with the evolving plasma is adjusted by changing the length of the optical path on the delay line.

The spatial distribution of the electron beam ejected from the gas jet is directly detected by a phosphor screen (DRZ), which is set at the rear of the gas jet [2]. The DRZ is sensitive to high energy particles and radiations, and is set 150 mm away from the focus point behind the 300 μm titanium foil; the exposure to x-rays, low energy electrons, and the laser pulses is eliminated.

The energy spectrum of the electron beam is detected by a magnetic electron deflector, which is set in the laser axis between the gas jet and the DRZ screen; see details in Ref. [2]. This setup allows detecting the energy spectrum of the electron beam from 7 to 60 MeV. Total charge of the electron beam is measured by an integrated current transformer (ICT), which is set at the laser axis behind the gas jet. We also perform the 2D particle-in-cell simulation by FPLaser2D code [5] to understand the process of the electron acceleration.

The transition radiation is generated at the rear of a 300 μm thick Ti foil. The radiation from the rear side of the foil is focused through a high-pass spectral filter ($\lambda <$ 50 μm or $\lambda < 100$ μm) to a bolometer by a system of parabolic mirrors as seen in Fig. 1. The cryogenic silicon bolometer (Infrared Laboratories Inc.) operating at 4.2 K temperature with the noise equivalent power less than 10^{-13} W/Hz$^{1/2}$ is equipped by set of 4 spectral low-pass filters transmitting the radiation with $\lambda > 28$ μm, >50 μm, >100 μm, and >280 μm, respectively, and several mesh high-pass filters.

The spectral intensity of THz transition radiation produced by an electron bunch strongly depends on the bunch length [9,10]:

$$P_{\mathrm{TR}}(\lambda) = n[1 + nf(\lambda)]P_e(\lambda), \tag{1}$$

where n is the number of electrons in a bunch,

$$f(\lambda) = \left| \int S(z) \exp(i2\pi z/\lambda) dz \right|^2 \tag{2}$$

is the bunch form factor with $S(z)$ the one-dimensional density distribution function;

$$P_e(\lambda) = \frac{\alpha\beta^2 \sin^2\theta \cos^2\theta}{\pi^2\lambda(1 - \beta^2\cos^2\theta)^2} |\zeta|^2 d\Omega d\lambda; \qquad \beta = v/c, \tag{3}$$

where α is the fine-structure constant, λ the wavelength, θ the direction angle from the electron beam axis, ε the permittivity of the metal, Ω the solid angle in the θ direction;

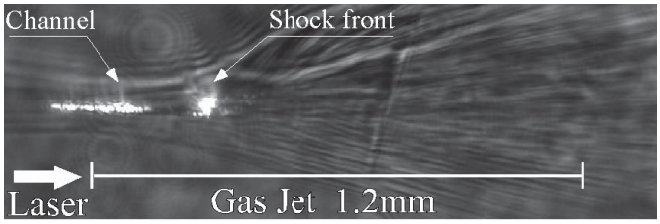

FIG. 2. Plasma shadowgraph image. The channel in the preplasma is produced by the laser prepulse.

$$\zeta = \frac{(\varepsilon - 1)[1 - \beta^2 - \beta(\varepsilon - \sin^2\theta)^{1/2}]}{[\varepsilon\cos\theta + (\varepsilon - \sin^2\theta)^{1/2}][1 - \beta(\varepsilon - \sin^2\theta)^{1/2}]}. \tag{4}$$

This equation is used to calculate the spectrum of the THz radiation. One can see that for the wavelength λ longer than the typical bunch length the intensity is proportional to n^2—the coherent radiation; in the opposite case the intensity is small, $\sim n$—incoherent. In contrast to $P_e(\lambda)$, the form factor $f(\lambda)$ strongly depends on the radiation wavelength that can be detected.

In the condition when the laser prepulse produces a plasma channel before the main pulse, as seen from the shadowgraph image in Fig. 2, relatively stable, low emittance electron beams are generated with a good reproducibility. Figure 3 shows spatial distributions of the electron deflected by a magnetic electron deflector and the energy spectrum; (a) and (b) with quasimonoenergetic distribution, (c) with Maxwell-like energy distribution, respectively. A typical image of the low emittance electron beam on the DRZ plate is shown in Fig. 3(a1). The emittance is estimated to be 0.07π mm mrad. The energy spectrum of the beam given in Fig. 3(a2) shows that the energy of the quasimonoenergetic electron beam is improved by factor 2 compared to our previous report [2]; the mean energy of the electrons is $\langle E\rangle = 21$ MeV with the energy spread $\Delta E \sim 4$ MeV ($\sim 20\%$). The total charge of the electron estimated via ICT measurement is about 100 pC. To determine the charge in the narrow range $\Delta E =$ 19–23 MeV where the electrons constitute a monoenergetic distribution, we use the results of PIC simulation. However, we also have obtained another electron bunch with spatial and energy distributions as shown in Figs. 3(b1) and 3(b2) with the same experimental conditions as Figs. 3(a1) and 3(a2). The peak energy and the energy spread have changed shot by shot due to shot-to-shot instability of laser and plasma parameters. For the channel with the minimal density $N_{\mathrm{emin}} = 1 \times 10^{19}$ cm^{-3}, the maximal density $N_{\mathrm{emax}} = 4 \times 10^{19}$ cm^{-3}, and the diameter $D = 20$ μm, we get the distribution that is very close to the experimental one as seen in Fig. 4(a). The

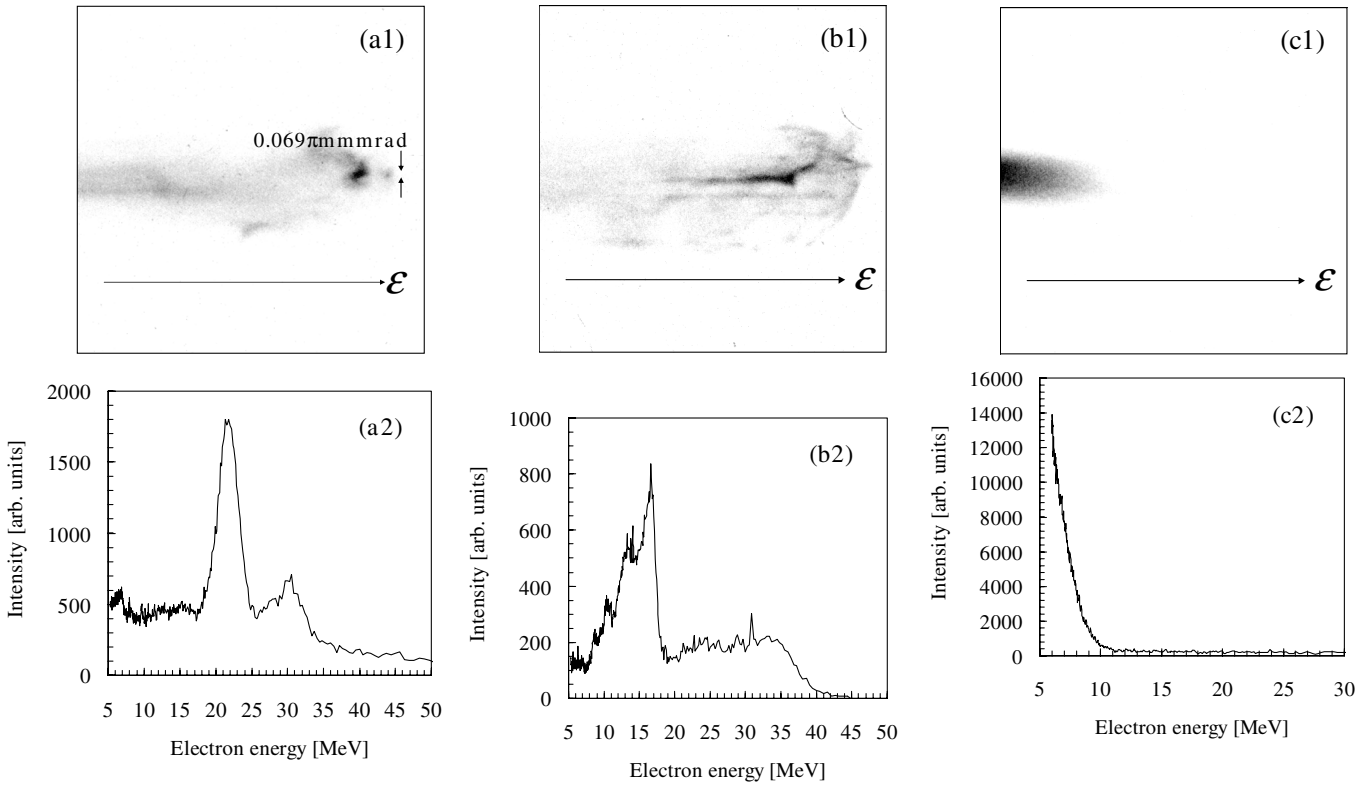

FIG. 3. Spatial distributions of the electron deflected by a magnetic electron deflector and the energy spectrum: (a) and (b) with quasimonoenergetic distribution; (c) with Maxwell-like energy distribution, respectively.

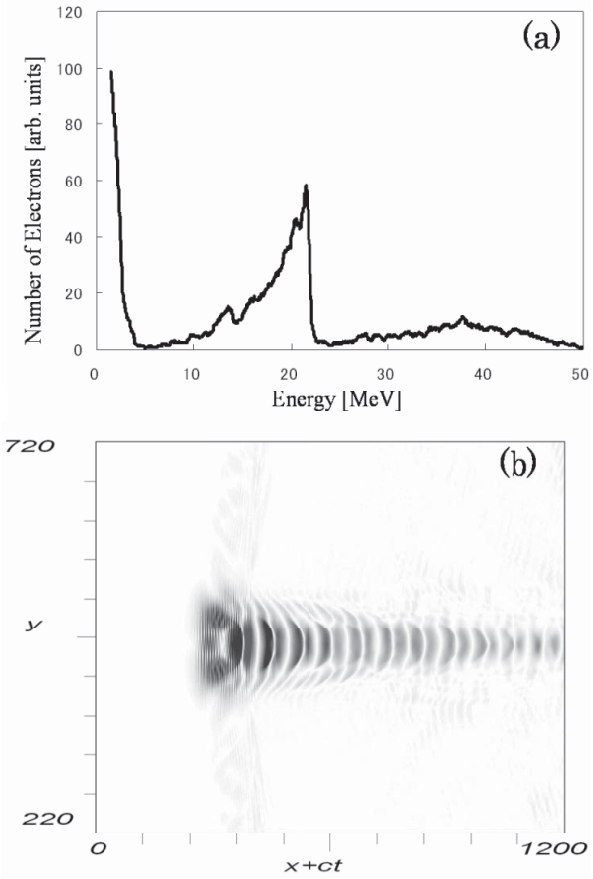

FIG. 4. (a) Energy distribution of the electron bunch and (b) spatial distribution of the longitudinal component of electric field of the plasma wave, in PIC simulation.

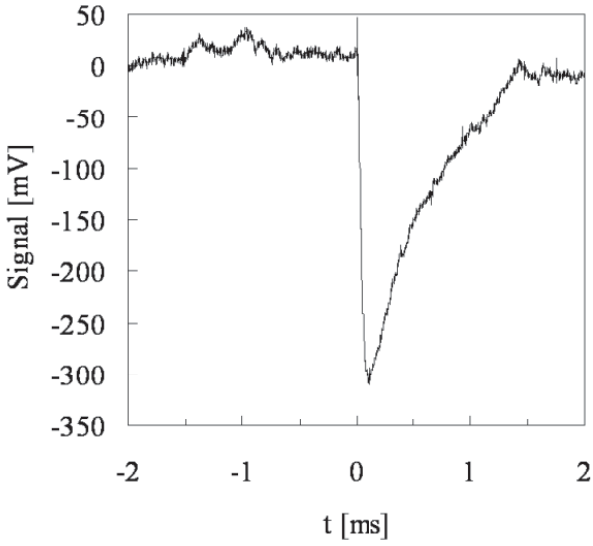

FIG. 5. Optimal signal form detected by the bolometer with a spectral low-pass filter of $\lambda > 100\ \mu$m. Its gap at $t = 0$ is proportional to the number of photons detected.

typical distribution of the plasma field is presented in Fig. 4(b). After normalizing the distribution function, we calculate the electron charge in the range; it is about 30 pC. This charge is big enough to produce a detectable signal of the transition radiation.

An optimal signal form detected by the bolometer with a spectral low-pass filter of $\lambda > 100\ \mu$m is shown in Fig. 5 and its gap at $t = 0$ is proportional to the number of photons detected. The results of spectral measurements of the transition THz radiation are presented in Fig. 6. The circles show averaged signals of the transition radiation generated from (a) quasimonoenergetic distributions peaked around 20 MeV, (b) quasimonoenergetic distribu-

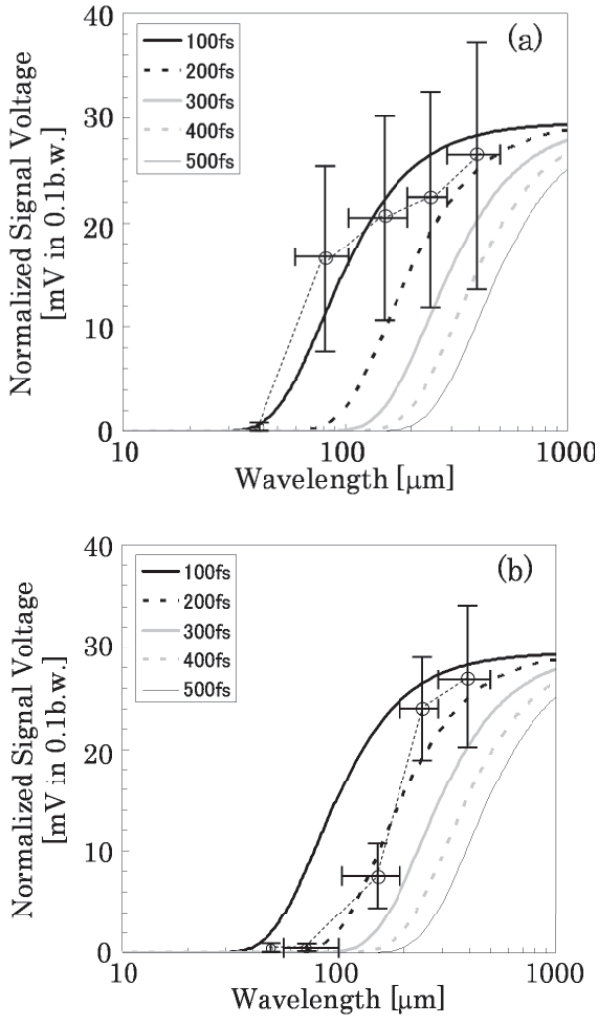

FIG. 6. Spectra of the transition radiation measured by a bolometer, generated from (a) quasimonoenergetic distributions peaked around 20 MeV, (b) quasimonoenergetic distributions peaked around 4 MeV. The circles show averaged signals of the transition radiation, placed at the middle of the detection ranges (determined by bandpass filters) shown by the horizontal error bars, and the vertical error bars describe these standard deviations. The calculated spectra of the transition radiation for different bunch duration are also included.

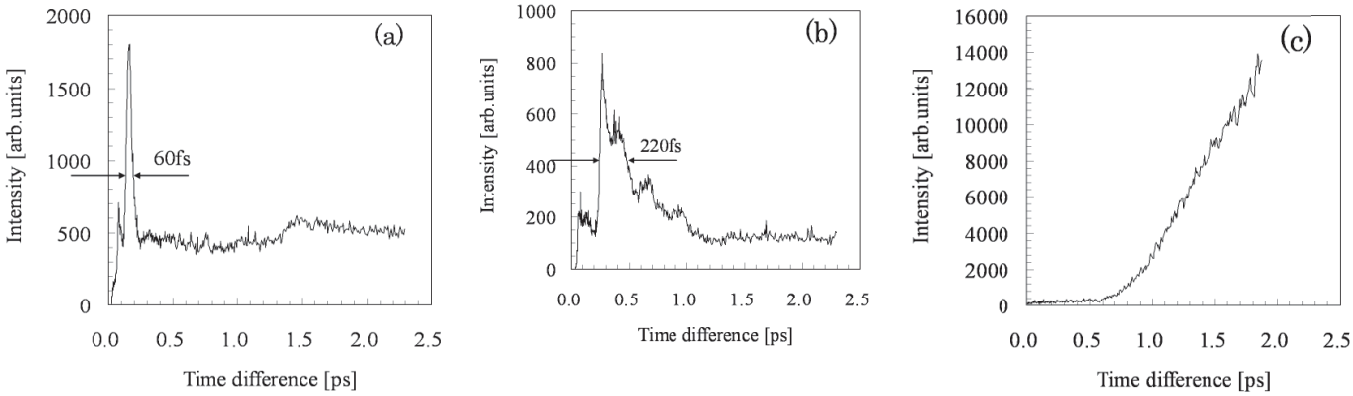

FIG. 7. Pulse elongation of the electron bunches: (a), (b) and (c) with the energy distributions as in Figs. 3(a2), 3(b2), and 3(c2), respectively, after 180 mm path, supposing initial bunch duration to be zero at the gas-jet rear.

tions peaked around 4 MeV, placed at the middle of the detection ranges (determined by the bandpass filters) shown by the horizontal error bars, and the vertical error bars describe these standard deviations. Along with the results, the calculated spectra of the transition radiation with use of Eq. (1) for different duration of a monoenergetic electron bunch are given. According to the calculated spectra, we can define the averaged duration of the high quality bunch as 130 ± 30 fs (FWHM), while it is 250 ± 70 fs (FWHM) for the low quality bunch. These are durations of the bunch after it propagates 180 mm behind the gas jet. Since the electron energy distribution has 100% dispersion in the Maxwell-like or about 20% dispersion even in the quasimonoenergetic, the bunch duration becomes longer. The durations are still almost equal to the top value of an electron bunch generated from a traditional radio-frequency linear accelerator: 240 fs (FWHM) at the S-band linac of University of Tokyo or from a SASE-FEL: 100 fs (FWHM) at DESY in Germany [10–12]. Assuming the energy spread, we can restore the initial duration of the electron bunch. In Figs. 7(a)–7(c), pulse elongation of the electron bunches with the energy distributions as in Figs. 3(a2), 3(b2), and 3(c2), respectively, is presented. Supposing initial bunch duration to be zero at the gas-jet rear, the pulse elongation of the quasimonoenergetic electron bunch after 180 mm path is ~60–220 fs (FWHM). Therefore, the initial duration of the electron bunch at the gas-jet rear is expected to be less than 100 fs (FWHM).

In conclusion, a quasimonoenergetic electron beam with its mean energy $E = 21$ MeV, dispersion $\Delta E = 4$ MeV, total charge $q \sim 30$ pC, and the geometrical emittance 0.07π mm mrad has been generated by the laser wakefield acceleration with high reproducibility. The bunch duration has been determined via direct spectral measurements of the coherent transition radiation. Because of the energy spread, the averaged duration of the bunch has been found to be 130 ± 30 fs (FWHM) for the quasimonoenergetic distributions peaked around 20 MeV and 250 ± 70 fs (FWHM) for the quasimonoenergetic distributions peaked around 4 MeV, respectively, at the distance 180 mm far from the gas jet. The initial duration of the electron bunch at the gas-jet rear is expected to be less than 100 fs (FWHM) at present. As the next step, we will perform a single-shot measurement using a polychromator to obtain more precise durations of electron bunch at the gas-jet rear very soon. We anticipate that such beams can be used for the femtosecond pump-probe analysis of condense matter.

[1] S. P. D. Mangles *et al.*, Nature (London) **431**, 535 (2004); C. G. R. Geddes *et al.*, *ibid.* **431**, 538 (2004); J. Faure, Y. Glinec, A. Pukhov, S. Kiselev, S. Gordienko, E. Lefebvre, J. P. Rousseau, F. Burgy, and V. Malka, *ibid.* **431**, 541 (2004); K. Koyama, E. Miura, S. Kato, N. Saito, S. Masuda, and M. Adachi, J. Particle Accel. Soc. Jpn. **1**, 158 (2004); A. Yamazaki *et al.*, Phys. Plasmas **12**, 093101 (2005); V. Malka, J. Faure, Y. Glineck, A. Pukhov, and J.-P. Rossean, Phys. Plasmas **12**, 056702 (2005); M. Kando *et al.*, Phys. Rev. E **71**, 015403(R) (2005).

[2] T. Hosokai, K. Kinoshita, A. Zhidkov, K. Nakamura, T. Watanabe, T. Ueda, H. Kotaki, M. Kando, K. Nakajima, and M. Uesaka, Phys. Rev. E **67**, 036407 (2003); T. Hosokai *et al.*, Phys. Plasmas **11**, L57 (2004); T. Hosokai *et al.*, Phys. Rev. E **73**, 036407 (2006).

[3] R. Neutze, R. Wounts, D. Spoel, E. Weckert, and J. Hajdu, Nature (London) **406**, 752 (2000); I. G. Gurthbay, J. M. Pitarke, and P. M. Echenique, Phys. Rev. B **69**, 245106 (2004); Y. Yang, N. Nogani, J. Shi, H. Chen, Y. Lin, and S. Quan, J. Appl. Phys. **98**, 033528 (2005); V. P. Zhukov, E. V. Chulkov, and P. M. Echenique, Phys. Rev. B **72**, 155109 (2005); W. E. King *et al.*, J. Appl. Phys. **97**, 111101 (2005).

[4] S. V. Bulanov, I. N. Inovenkov, V. I. Kirsanov, N. M. Naumova, and A. S. Sakharov, Phys. Fluids B **4**, 1935 (1992); S. V. Bulanov, F. Pegoraro, A. M. Pukhov, and A. S. Sakharov, Phys. Rev. Lett. **74**, 710 (1995); S. Bulanov, N. Naumova, F. Pegoraro, and J. Sakai, Phys. Rev. E **58**, R5257 (1998); S. V. Bulanov, M. Yamagiwa, T. Zh. Esirkepov, J. K. Koga, M. Kando, Y. Ueshima, and K. Saito, Phys. Plasmas **12**, 073103 (2005); F. S. Tsung,

P. Narang, W. B. Mori, C. Joshi, R. A. Fonseca, and L. O. Silva, Phys. Rev. Lett. **93**, 185002 (2004); D. F. Gordon, R. F. Hubbard, J. N. Cooley, B. Hafizi, A. Ting, and P. Sprangle, Phys. Rev. E **71**, 026404 (2005); C. B. Schroeder, E. Esarey, B. A. Shadwick, and W. P. Leemans, Phys. Plasmas **13**, 033103 (2006).

[5] A. Zhidkov, J. Koga, T. Hosokai, K. Kinoshita, and M. Uesaka, Phys. Plasmas **11**, 5379 (2004); A. Zhidkov, J. Koga, K. Kinoshita, and M. Uesaka, Phys. Rev. E **69**, 035401 (2004); T. Ohkubo, A. Zhidkov, T. Hosokai, K. Kinoshita, and M. Uesaka, Phys. Plasmas **13**, 033110 (2006).

[6] T. Tajima and J. M. Dawson, Phys. Rev. Lett. **43**, 267 (1979).

[7] J. van Tilborg, C. B. Schroeder, C. V. Filip, Cs. Toth, C. G. R. Geddes, G. Fubiani, R. Huber, R. A. Kaindl, E. Esarey, and W. P. Leemans, Phys. Rev. Lett. **96**, 014801 (2006); W. P. Leemans, J. van Tilborg, J. Faure, C. G. R. Geddes, Cs. Toth, C. B. Schroeder, E. Esarey, G. Fubiani, and G. Dugan, Phys. Plasmas **11**, 2899 (2004).

[8] S. Barerjee, S. Sepke, R. Shah, A. Valenzuela, A. Maksimchuk, and D. Umstadter, Phys. Rev. Lett. **95**, 035004 (2005).

[9] Y. Shibata, K. Ishi, T. Takahashi, T. Kanai, F. Arai, S. Kimura, T. Ohsaka, and M. Ikezawa, Phys. Rev. E **49**, 785 (1994); Y. Shibata, T. Takahashi, T. Kanai, K. Ishi, M. Ikezawa, J. Ohkuma, S. Okuda, and T. Okada, *ibid.* **50**, 1479 (1994); M. Uesaka *et al.*, Nucl. Instrum. Methods Phys. Res., Sect. A **410**, 424 (1998); P. Kung, H. Lihn, and H. Wiedemann, Phys. Rev. Lett. **73**, 967 (1994).

[10] T. Watanabe *et al.*, Nucl. Instrum. Methods Phys. Res., Sect. A **437**, 1 (1999); T. Watanabe *et al.*, *ibid.* **480**, 315 (2002).

[11] M. Uesaka *et al.*, IEEE Trans. Plasma Sci. **28**, 1133 (2000); *Femtosecond Beam Science*, edited by M. Uesaka (Imperial College Press, London, 2005).

[12] E. L. Saldin, E. A. Schneidmiller, and M. V. Yurkov, Opt. Commun. **239**, 161 (2004).